Water Supply

IWA PUBLISHING

Water Supply Vol 23 No 12, 4976 doi: 10.2166/ws.2023.313

Effect of field of view of canopy temperature observations on crop water stress index for irrigation scheduling

Aditi Yadav*, Hitesh Upreti and Gopal Das Singhal

Department of Civil Engineering, Shiv Nadar Institution of Eminence, Greater Noida, UP, India
*Corresponding author. E-mail: ay453@snu.edu.in

ABSTRACT

The monitoring of canopy temperature (T_c) helps to establish appropriate watering methods. This study calculates the crop water stress index (CWSI) for four irrigation regimes in semi-arid region, India. Plots 1, 2, 3, and 4 had soil moisture depletion of 50% (drip system), 25% (drip system), unregulated (farmer replicated flood system), and 50% (flood system) with irrigation. In this work, we examined the value of employing a portable infrared thermometer (IRT) to measure wheat canopy temperature (T_c) at two geographical locations. The IRT field of view is 51.28–5,128 cm^2, or 10–100 cm from the canopy crown. The field of view change from 10 to 100 cm affects T_c and CWSI in the four irrigation treatments, ranging from 0.65 to 2.71% and 9.2 to 36.4%, respectively. The research found that increasing the IRT from 10 to 100 cm reduced slope by 5.7% and intercept by 20.6% in lower baselines. The R^2 for CWSI and soil moisture was 0.78 (10 cm) and 0.77 (100 cm). Drip-irrigated plots are more sensitive to IRT spatial resolution than flood-irrigated plots. The findings suggest that CWSI studies may benefit from specific sample methods for T_c evaluation.

Key words: canopy temperature, drip irrigation, flood irrigation, irrigation scheduling, wheat

HIGHLIGHTS

- Drip-irrigated (DI) plots give lesser CWSI as compared to flood-irrigated (FI) plots.
- DI plots are more sensitive to the location of the infrared thermometer (IRT) than FI plots.
- The highest change in canopy temperature (T_c) and CWSI was observed in the most frequently irrigated DI plot.
- The work highlights the impact of change in the field of view of IRT on T_c, lower baselines, and CWSI.
- Relationship between CWSI and soil moisture studied.

GRAPHICAL ABSTRACT

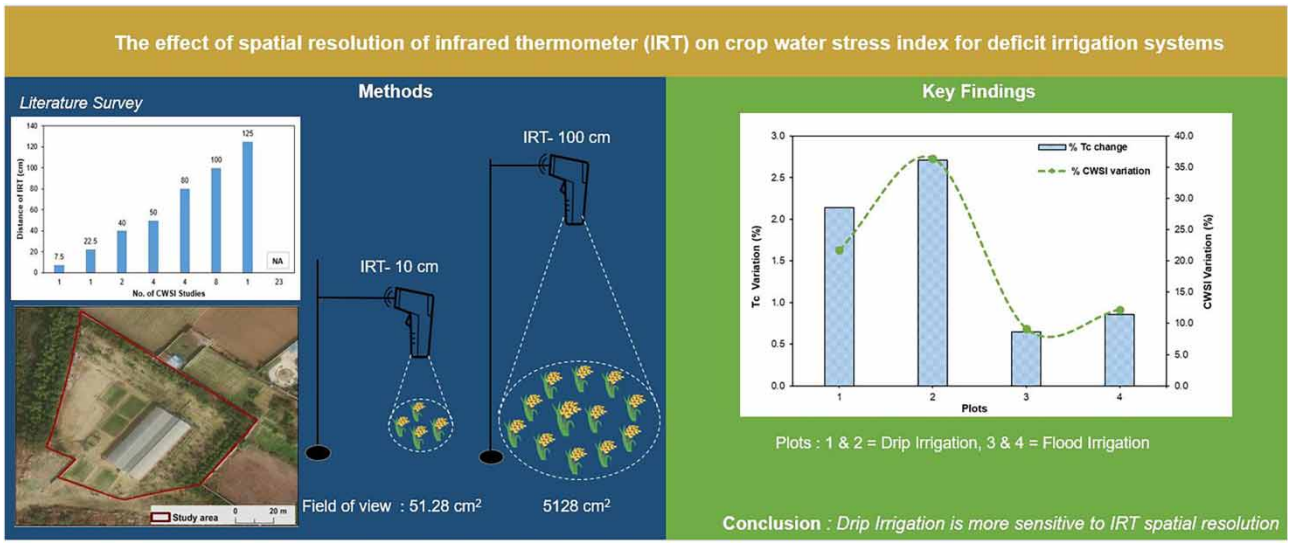

1. INTRODUCTION

Rapid climate change and industrialization are leading to an imbalance in the demand for and supply of limited freshwater supplies. Agriculture uses 70% of the world's freshwater resources (Shankar *et al.* 2013) placing tremendous stress on the agriculture industry. Notably, the per-acre yields from irrigated agriculture are twice as much as those from rain-fed agriculture (The World Bank Report 2020). Efficient water management in agriculture, particularly through irrigation, has emerged as a viable strategy to optimize crop water consumption while maintaining productivity. Such efforts are pivotal in achieving sustainable agriculture and aligning with the United Nations Sustainable Development Goal 2 (SDG 2: Zero Hunger), which underscores the importance of developing effective irrigation schedules (UN 2022). Research studies on efficient farm water management have been conducted globally (Akuraju *et al.* 2021; Jamshidi *et al.* 2021; King *et al.* 2021; Gölgül *et al.* 2022).

There are two major approaches for designing irrigation schedules in agriculture for optimum water management. They are (a) soil-based methods such as soil moisture estimation reflecting soil water status and (b) plant-based methods, such as leaf water potential, stomatal opening, transpiration, and canopy temperature reflecting plant water status. Plant-based approaches are more accurate in the development of irrigation schedules because they provide a comprehensive perspective of the interplay between soil, plant, and environment. The pressure chamber method is commonly used to monitor the stem water potential and leaf water potential of plants, but it has some drawbacks, such as complex operation, destructive, time-consuming, and laborious characteristics that make it unsuitable for long-term monitoring of plant water status. In plant-based approaches, an alternate method is the canopy temperature assessment, which is a simple operation and a non-destructive method to assess the plant water status.

With advancements in remote sensing equipment, infrared thermometers (IRT) have gained prominence in agricultural research. Canopy temperature (T_c), recorded by IRT, has been widely utilized to determine optimal irrigation timing (Yuan *et al.* 2004; Li *et al.* 2010; Bellvert *et al.* 2014; Taghvaeian *et al.* 2014; Çolak *et al.* 2015). IRTs, available in various models (hand-held, mounted, commercial, and research-grade), collect data in the spectral range of 8–14 μm and provide canopy temperature readings within their field of view.

Stress degree days (SDD), which is the difference between canopy and air temperature (Jackson *et al.* 1977; Idso *et al.* 1981; Romero-Trigueros *et al.* 2019), is used to generate a plant-based indicator known as crop water stress index (CWSI). The CWSI was first derived by Idso *et al.* (1981). Two popular methods, empirical (Idso *et al.* 1981) and theoretical (Jackson *et al.* 1981), can be used to determine CWSI. Out of the two, the empirical approach has a wider range of applications (Idso 1982; Jalali-Farahani *et al.* 1993; Usman *et al.* 2009; Taghvaeian *et al.* 2012; Kumar *et al.* 2019; Ru *et al.* 2020) owing to its simplistic nature. The empirical CWSI uses three predictors: air temperature (T_a), relative humidity (RH), and canopy temperature (T_c), wherein two critical SDDs termed lower baseline and upper baseline are further formulated for its development. The lower and upper baselines are derived by regressing the SDD with a vapor pressure deficit (VPD) under conditions of maximum water in the root zone leading to maximum evapotranspiration and minimum water in the root zone leading to minimum evapotranspiration, respectively (Idso *et al.* 1981; Gontia & Tiwari 2008; Kumar *et al.* 2019; Ru *et al.* 2020).

The primary variables T_a, RH, and T_c are measured *in situ* using various sensors for the evaluation of empirical CWSI. T_a and RH are measured on-site at meteorological stations (automated weather stations (AWS)) (Alghory & Yazar 2019; Kumar *et al.* 2019; Romero-Trigueros *et al.* 2019; Shellie & King 2020). While studying the T_a and RH observations, the sensors of AWS were placed 1.5–2 m above the ground (Idso *et al.* 1981; Idso 1982; Payero & Irmak 2006; Kar & Kumar 2010; Han *et al.* 2018; Alghory & Yazar 2019; Shellie & King 2020; Jamshidi *et al.* 2021; King *et al.* 2021).

Prior to the introduction of IRT, T_c measurements were made using mercury thermometers (Ehlers 1915) and thermocouples (Miller & Saunders 1923). Many research investigations have used IRT for effective T_c observation since its inception (Alderfasi & Nielsen 2001; Kar & Kumar 2007, 2010; Akuraju *et al.* 2021; Khorsand *et al.* 2021). However, while researching the use of hand-held IRT in the literature, the distance at which the hand-held IRT is aimed towards the canopy reveals a wide variety of distances. T_c sensing distances have been reported to be 5–10 cm (Ru *et al.* 2020), 15–30 cm (Shellie & King 2020), 50 cm (Romero-Trigueros *et al.* 2019; King *et al.* 2021), 80 cm (Han *et al.* 2018), and 100 cm (Payero & Irmak 2006; Bellvert *et al.* 2014; Çolak *et al.* 2021; Jamshidi *et al.* 2021).

Given that CWSI is widely used in irrigation scheduling studies (Garrot Jnr *et al.* 1994; Gontia & Tiwari 2008; Erdem *et al.* 2010; Kirnak *et al.* 2019; Kumar *et al.* 2019), reliable CWSI values are critical. The correctness of the input variables of T_a, RH and T_c is crucial for the same. However, as noted in the preceding section, T_a and RH are generally measured at a constant distance using on-site sensors; however, the distance at which portable IRT devices are oriented towards the canopy varies

significantly in the literature. For example, research has positioned IRT from the crown at distances ranging from 5–10 cm to 100 cm, with many studies not specifying the IRT distance. A comprehensive literature survey of the distances at which IRT was maintained in various CWSI studies is presented in Section 2. This unexplained variation in IRT observation distance raises concerns regarding the influence on empirical CWSI values.

This study is undertaken to understand the effect of IRT distances on the empirical CWSI values. Specifically, we investigate two distances – 10 and 100 cm – from the top of the crown (at the nadir view). The study analyzes the sensitivity to the observation distance of IRT of the following variables:

(a) canopy temperature (T_c);
(b) the slope and intercept of lower baselines;
(c) CWSI values;
(d) the determination coefficient (R^2) between CWSI and soil moisture depletion.

Additionally, we explore how changes in the spatial resolution of the remote sensing device, IRT, affect two types of irrigation systems: drip irrigation and flood irrigation. It quantifies the impact the location of an instrument (IRT) has on different parameters associated with CWSI estimation. As far as the authors are aware, no prior study investigating the significance of IRT observation distances were identified during the literature review phase of this investigation. This research can serve as a foundation for developing IRT-based T_c measurement guidelines.

2. MATERIALS AND METHODS

2.1. Study area and experimental plot details

Controlled irrigation experiments on wheat crops in sandy loam soil were performed at the Water Management Field laboratory, on the campus of the Shiv Nadar Institution of Eminence (SNIoE) in Greater Noida, Uttar Pradesh, India. According to the Koppen–Geiger climate classification system, the study area has a humid subtropical climate (Cwa) (Kottek *et al.* 2006). During the wheat crop duration of 120 days for the experimental season 2021–2022, the average daily means of air temperature, relative humidity, wind speed, incoming solar radiation, and total rainfall are 17.23°, 69.55%, 0.47 m/s, 149.05 W/m^2, and 100.5 mm, respectively.

The DBW 173 wheat crop was planted on 16 December 2021, and it was harvested on 15 April 2022. The plan for the study includes four different irrigation treatments in field plots numbered 1, 2, 3, and 4 which are, each of size 25 m^2. Each plot has been given four replications. The analysis has been conducted over a total of 16 plots.

Drip irrigation was applied to plots 1 and 2 at soil moisture depletion levels of 50 and 25%, respectively. Each of the two drip-irrigated (DI) plots consisted of 21 pipes with 30 drip nozzles from each pipe, supplying water directly to the root zone of wheat crops. Treatment with flood irrigation was applied to plots 3 and 4. The irrigation schedule for plot 3 was based on the general irrigation guidelines for a typical farmer's field in the area, which is an application of a fixed amount of water at a fixed interval, whereas, plot 4 received flood irrigation at a soil moisture depletion of 50%.

2.2. Equipment

The sensors mounted on AWS are stationed at a height of 2 m above the ground. AWS collects meteorological data on air temperature, relative humidity, wind speed, and incoming solar radiation with a temporal resolution of 15 min every day. The tipping bucket-type rain gauge (stationed within the study area) recorded the total rainfall. A profile probe for soil moisture (PR2/6) from Delta-T Devices (Figure 1(a)) has been used to measure the soil moisture in all the plots. To measure the temperature of the canopy (T_c), a hand-held infrared thermometer (IRT) (Apogee Instruments, model MI-211) was employed. It has a 22° field of view at a half angle and can detect infrared radiation in the 8–14 μm band. IRT was kept at a distance of 10 and 100 cm from the top of the crown (with a nadir view) to estimate two T_c values in each plot. IRT readings were taken at 12:00–14:00 h. Figure 1 shows the equipment used for this study.

2.3. Methods

A detailed literature survey was conducted over a wide variety of crops to understand the most widely adapted observation distance of the IRT sensor for T_c recordings. The results are presented in Table 1. It was seen that the maximum number of studies (23) did not specify the T_c sensor distance. This lack of specification reflects the non-clarity in the T_c sampling procedure for CWSI estimations studies.

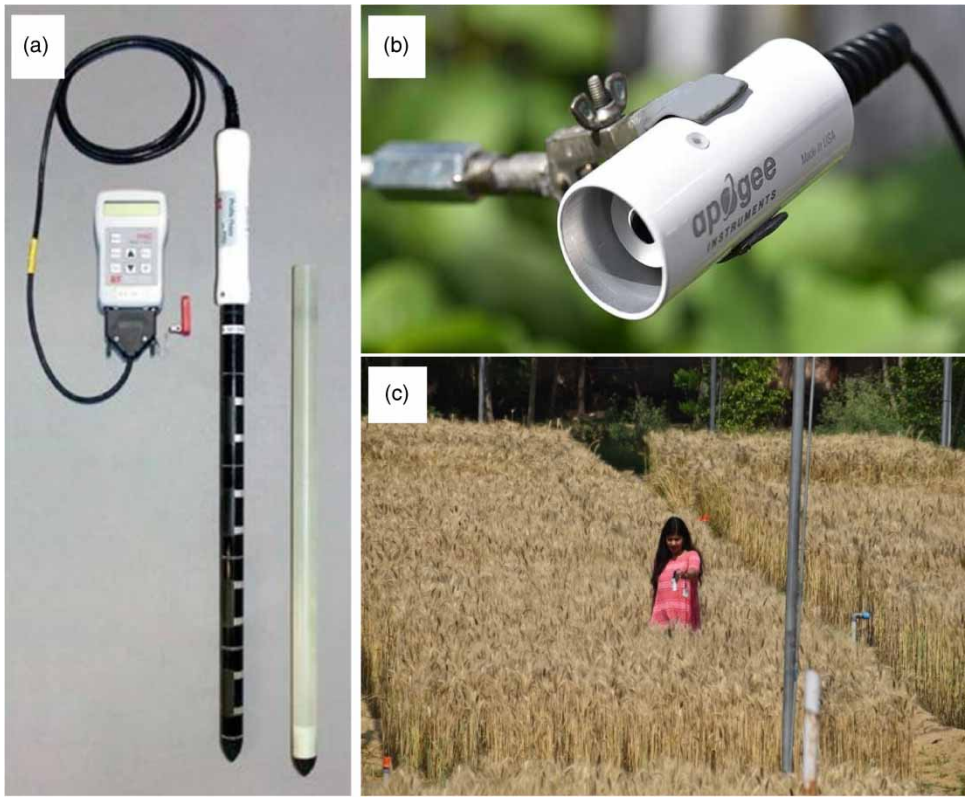

Figure 1 | (a) Soil moisture profile probe with data logger (PS 2/6), (b) infrared thermometer (MI-211), and (c) on-site data collection of canopy temperature of wheat using IRT.

Table 1 | Literature survey of distance of infrared thermometer (IRT) from canopy surface for various crop varieties

Distance of IRT from canopy (in cm)	Number of studies	References
5–10	1	Ru *et al.* (2020)
15–30	1	Shellie & King (2020)
30–50	2	Usman *et al.* (2009) and Adeyemi *et al.* (2018)
50	4	Jalali-Farahani *et al.* (1993), Orta *et al.* (2004), Romero-Trigueros *et al.* (2019), King *et al.* (2021)
80	4	Taghvaeian *et al.* (2012), Taghvaeian *et al.* (2014), Han *et al.* (2018), DeJonge *et al.* (2015)
100	8	Jackson *et al.* (1977), Payero & Irmak (2006), Bellvert *et al.* (2014), Taghvaeian *et al.* (2014), Çolak *et al.* (2015, 2021), Haghverdi *et al.* (2021), Jamshidi *et al.* (2021)
100–150	1	Alghory & Yazar (2019)
Not available	23	Idso *et al.* (1981), Idso (1982), Howell *et al.* (1986), Stegman & Soderlund (1992), Stockle & Dugas (1992), Garrot Jnr *et al.* (1994), Alderfasi & Nielsen (2001), Yuan *et al.* (2004), Kar & Kumar (2007, 2010), Gontia & Tiwari (2008), Erdem *et al.* (2010), Li *et al.* (2010), Bijanzadeh & Emam (2012), Paltineanu *et al.* (2013), Sneha *et al.* (2013), Irandoust & Bijanzadeh (2018), Kirnak *et al.* (2019), Kumar *et al.* (2019, 2020), Akuraju *et al.* (2021), Khorsand *et al.* (2021), Gölgül *et al.* (2022)

2.3.1. Canopy temperature (T_c) at 10 and 100 cm

Canopy temperature (T_c) has been observed for each plot beginning from the jointing phase (in which the wheat crop occupies 70% of the sown area) by pointing the IRT at the nadir view towards the canopy surface, at a distance of (i)

10 cm from the top of the crown and (ii) 100 cm from the top of the crown. In the first case, the IRT covers a canopy area of about 51.28 cm^2 (with a diameter of 8.08 cm), and in the second case, an area of 5,128 cm^2 (with a diameter of 80.82 cm). The 10 cm case and 100 cm case cover the wheat canopy surface of 1–2 plants and 25–30 plants, respectively. According to several studies, the daytime T_c is ideal for the measurement of CWSI (Jackson *et al.* 1977; Idso *et al.* 1981). For the same reasons, T_c measurements in this study were made at noon when the sun was directly overhead between 12:00 and 14:00 h.

2.3.2. Lower baselines and upper baselines

For the calculation of CWSI values, the design of two baseline conditions is crucial (Idso *et al.* 1981). The two baselines represent two critical conditions that result from the interaction of the plant, soil, and air continuums. The first critical baseline condition is commonly referred to as 'lower baseline' or 'non-water stressed baseline,' and it results from a linear relationship between SDD and VPD for the condition when the canopy is supplied with the most water, exposing it to the least amount of water stress and the highest evapotranspiration rate. The second critical baseline is referred to as the 'upper baseline' or 'maximum water-stressed baseline,' which represents the condition when the canopy suffers maximum water stress and the lowest evapotranspiration rate.

Plot 2, which received drip irrigation at 25% soil moisture depletion, provides the data for lower baseline design. The settings are good for non-water-stressed conditions, which helps design a lower baseline. Two lower baselines are designed for the two cases. Firstly, consider the case in which the canopy is viewed from a distance of 10 cm, and then consider the case in which the canopy is viewed from a distance of 100 cm. The upper baseline for the wheat crop is set at 2 °C (Idso *et al.* 1981; Howell *et al.* 1986; Alderfasi & Nielsen 2001; Orta *et al.* 2004; Yuan *et al.* 2004; Gontia & Tiwari 2008; Alghory & Yazar 2019).

2.3.3. Empirical CWSI values

Empirical CWSI values are calculated using the three predictors of T_a, T_c, and VPD (Idso *et al.* 1981). VPD is a function of T_a and RH. The mathematical representation of CWSI as per Idso *et al.* (1981) is as follows:

$$\mathrm{CWSI} = \frac{(T_c - T_a) - (T_c - T_a)_{LL}}{(T_c - T_a)_{UL} - (T_c - T_a)_{LL}} \tag{1}$$

where $(T_c - T_a)$ represents the observed SDD at the time of data collection. $(T_c - T_a)_{LL}$ and $(T_c - T_a)_{UL}$ represent the lower baseline and upper baseline, respectively. CWSI value of 0 is a representative of the minimum stress condition and the ratio of actual evapotranspiration to potential evapotranspiration at this point is 1. CWSI = 1 represents a maximum stress condition and the ratio of actual evapotranspiration to potential evapotranspiration of 0 (Idso *et al.* 1981). However, the maximum CWSI can exceed beyond 1 and below 0, while performing empirical CWSI calculations (Yuan *et al.* 2004; Gontia & Tiwari 2008; Li *et al.* 2010). The values of 0 and lesser than 0 represent the non-stressed condition of fully transpiring canopies (Gontia & Tiwari 2008). On the other hand, values of 1 and above 1 represent the severely stressed conditions of non-transpiring canopies (Li *et al.* 2010). Utilizing the lower baselines and canopy temperature devised for the two cases of 10 and 100 cm, the CWSI values for all the 16 plots have been estimated for noon time for the two cases, of IRT distance (i) 10 cm and (ii) 100 cm.

2.3.4. Evaluation criteria

For the analysis of the relationship between CWSI and soil moisture depletion (%), the statistical measure of coefficient of determination (R^2) was applied. R^2 is calculated using Equation (2):

$$R^2 = \frac{\left[\sum_{i=1}^{n} (Y_{o,i} - Y_{mo})(Y_{p,i} - Y_{mp})\right]^2}{\sum_{i=1}^{n} (Y_{o,i} - Y_{mo})^2 \sum_{i=1}^{n} (Y_{p,i} - Y_{mp})^2} \tag{2}$$

3. RESULTS AND DISCUSSIONS

3.1. Analysis of canopy temperature (T_c) at distances of 10 and 100 cm

In Figure 2(a), we present the average T_c values for all plots during the 2021–2022 wheat crop study season. Notably, when measuring T_c at distances of 10 and 100 cm, we observed distinct trends among the plots. Plot 2 exhibited the most significant increase in T_c at 2.71%, followed by plots 1 (2.14%), 4 (0.86%), and 3 (0.65%). Interestingly, we noted that regulated irrigation plots, such as plot 2, experienced the highest T_c fluctuations (2.71%), while unregulated irrigation plots, such as plot 3, showed the lowest T_c variations (0.65%) (Figure 2(a)).

These observations are attributed to the characteristics of the irrigation methods employed. DI plots (1 and 2) demonstrated the most substantial changes due to the inherent features of drip irrigation systems. In these plots, water is supplied uniformly at the root level but with uneven lateral soil wetting. As a result, soil moisture distribution directly under the plant is higher, gradually decreasing with distance from the plant (Figure 3). Conversely, flood-irrigated plots (3 and 4) displayed more even lateral soil wetting, leading to less pronounced T_c variations. This variation in soil temperature is reflected in the T_c values, especially when the IRT is placed at 100 cm, capturing multiple drip nozzles' effects and lateral uneven wetting.

Further, the crop stages are divided into three stages: pre-heading, anthesis, and grain filling. The pre-heading stage contains data from the jointing and boot leaf phases. The anthesis stage contains data from pollination and the flowering phases. The grain-filling stage contains the milking and dough phases of crop growth. An analysis of T_c variation upon taking the IRT sensor from a distance of 10 to 100 cm over the three crop stages can be seen in Figure 2(b). As shown in Figure 2(b), when the crop reaches its mature stage of grain filling, the variation in T_c values is highest. The pre-heading stage shows variations in T_c of 0.5, 0.55, 0.43, and 0.18 °C, at plots 1, 2, 3, and 4, respectively. The anthesis stage shows variations in T_c of 0.46, 0.38, and 0.23 °C for plots 1, 2, and 3, respectively. Here, plot 4 shows a negligible change. The grain filling stage shows a significant change in T_c of 0.69, 1.04, and 0.38 °C at plots 1, 2, and 4, respectively. Here, for plot 3, there is no significant change at this stage. The DI plots show maximum variation in the grain filling stage followed by pre-heading and anthesis stages. This behavior can be attributed to the plant's physiology, characterized by greater longitudinal growth than lateral growth during grain filling, resulting in the visibility of the unevenly moist soil pixels within the IRT's field of view when positioned 100 cm from the canopy, whereas during the anthesis stage the plant physiology covers the soil surface (both longitudinal and lateral growth) leading to lesser noise in the T_c dataset for a 100 cm field of view. In the pre-heading stage, the canopy is underdeveloped in its vegetative growth phase. This exposes the IRT to considerable soil pixels of the pre-heading phase. The flood-irrigated plots 3 and 4 show much lesser discrepancies in T_c values at 100 cm from 10 cm because of the involvement of uniformly wetted soil patches in the field of view of IRT sensors.

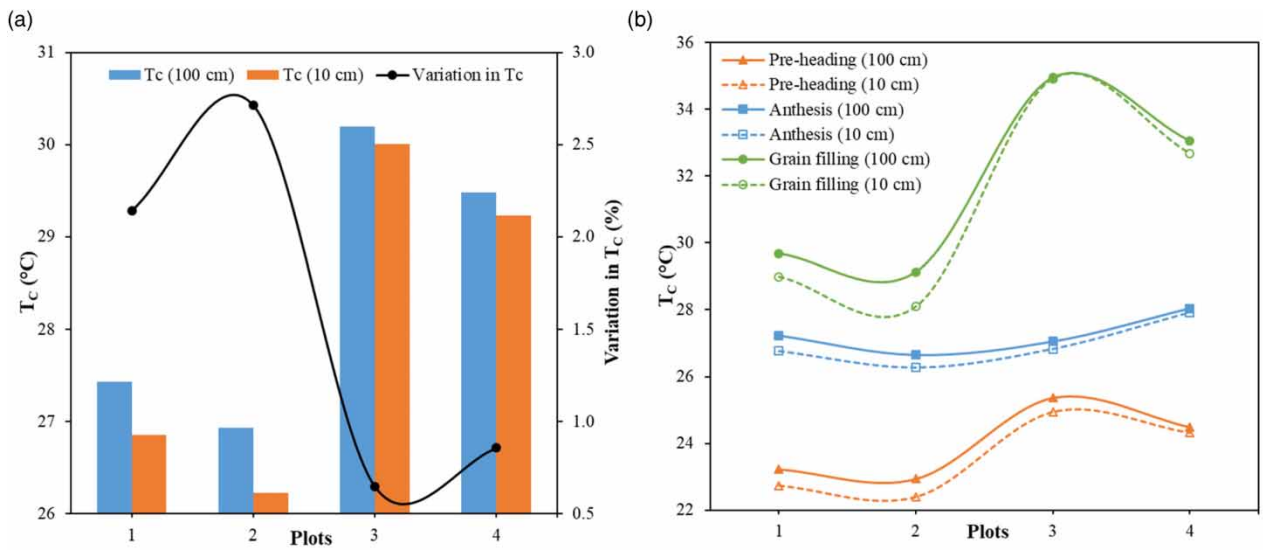

Figure 2 | Comparison of mean canopy temperature (T_c) values for various irrigation treatments for 10 and 100 cm: (a) full season and (b) three growth stages of wheat crop.

Figure 3 | The uneven wetting of soil due to drip nozzles in study area field plots 1 and 2.

After conducting a comparative analysis of T_c values at a distance of 10 cm throughout the three phases of crop growth, it was noted that there has been a consistent upward trend in the values of T_c likely due to increased solar radiation, as crop growth progresses through the months of February to March 2022. The measured increase in T_c from the pre-heading stage to the anthesis stage at a distance of 10 cm is 17.79, 17.36, 7.60, and 14.86% for plots 1, 2, 3, and 4, respectively. An increase in T_c of 8.30, 6.95, 30.11, and 17.01% has been detected in the growth rate from the anthesis to the grain filling stage for plots 1, 2, 3, and 4, respectively. In a similar vein, it was noted that there was a rise in T_c at a distance of 100 cm during the various phases of crop growth. Specifically, there was a reported increase of 17.26, 16.22, 6.69, and 14.51% from the pre-heading stage to the anthesis stage for plots 1, 2, 3, and 4, respectively. There has been an observed rise of 8.99, 9.30, 29.23, and 17.90% in the growth stages from anthesis to maturity for plots 1, 2, 3, and 4, correspondingly. The findings indicate that the T_c of flood-irrigated plots demonstrates greater sensitivity to changes in the crop development stage, namely from the anthesis to the maturity stage, as compared to the DI plots. Conversely, DI plots exhibited higher sensitivity during the transition from pre-heading to anthesis. Additionally, it can be noted that an increase in T_c at 10 cm from pre-heading to anthesis is equivalent in magnitude to an increase in T_c at 100 cm for the same growth stage transition for a particular plot. The similarity can be noted across different stage transitions from 10 to 100 cm of T_c variation under all plots.

These findings collectively contribute to a better understanding of how irrigation methods, crop growth stages, and IRT location affect T_c variations, offering valuable insights for optimizing crop management and irrigation practices.

3.2. Analysis of lower baselines at distances of 10 and 100 cm

The non-stressed baseline or lower baseline for the distances of 10 and 100 cm is shown in Figure 4. The linear relationship between SDD (i.e. $T_c - T_a$) and VPD has a better correlation value of $R^2 = 0.83$ for the 10 cm case than the R^2 value of 0.77 for the 100 cm case. The equations for lower baselines for the cases of 10 cm (Equation (3)) and 100 cm (Equation (4)) are shown as follows:

$$T_c - T_a = -1.29(\text{VPD}) - 2.19 \tag{3}$$

$$T_c - T_a = -1.21(\text{VPD}) - 1.74 \tag{4}$$

Moving the IRT from a 10 cm observation distance to a 100 cm observation distance resulted in a noticeable 5.7% decrease in slope and a substantial 20.6% decrease in the intercept value of the lower baseline. Particularly, we focused on the

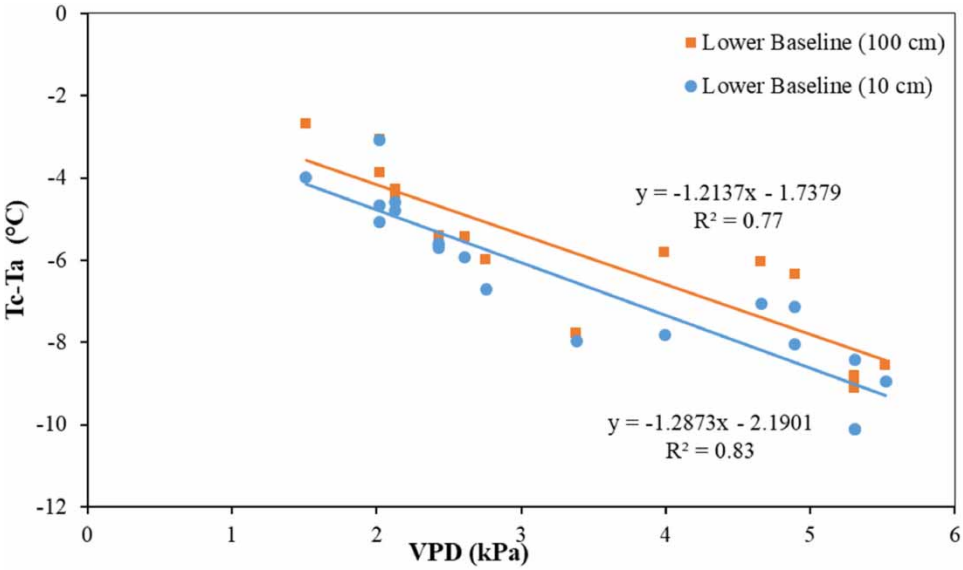

Figure 4 | Lower baselines for 10 and 100 cm.

non-water-stressed treatment in plot 2, which played a crucial role in establishing a lower baseline for this experiment. Intriguingly, this treatment exhibited the highest variation, with CWSI readings fluctuating by 36.0% for a relatively modest 2.7% change in T_c (Figure 5). As a result, we observed significant alterations in lower baseline readings when transitioning from 10 to 100 cm observation distances.

The IRT's observation distance for research in wheat crop studies demonstrates a range of observation distances. For instance, Alghory & Yazar (2019) have estimated lower baselines, with slope and intercept of −1.22 and 0.49 from the IRT sensor located at 1–1.5 m, whereas Orta *et al.* (2004) deduced the lower baselines, with slope and intercept of 1.35 and 0.63 at a distance of 0.5 m. The slope and intercept values, respectively, of lower baselines of other studies that have not clearly quantified the distance of the IRT sensor from the crop canopy, are as follows: −1.11 and −2.08 (Gontia & Tiwari 2008), −1.5 and 0.41 (Alderfasi & Nielsen 2001), −1.5 and 1.36 (Yuan *et al.* 2004), −1.41 and 2.89 (Bijanzadeh & Emam 2012), −1.29 and 1.54 (Howell *et al.* 1986), and −1.10 and −3.77 (Kar & Kumar 2010).

When these values of the lower baselines from different climate conditions are compared with the values of the lower baseline at 10 cm of our study area with a sub-humid tropical climate, the observed variation in slope and intercept, respectively, are as follows: the sub-humid subtropical region of Khargapur, India has 13.64 and 4.89% (Gontia & Tiwari 2008), the cold semi-arid region of Fort Collins, USA has 16.28 and 81.28% (Alderfasi & Nielsen 2001), semi-arid region of Tekirdag, Turkey

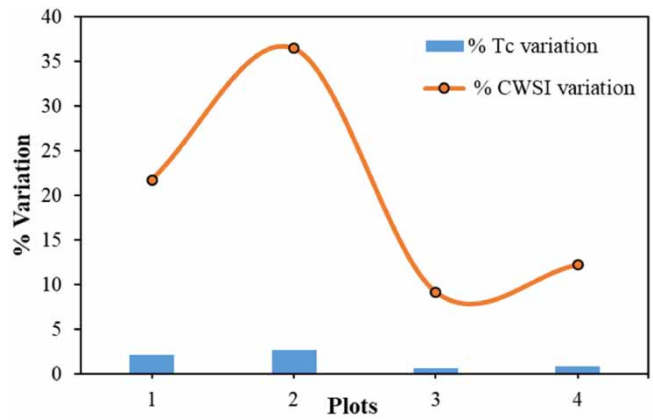

Figure 5 | The variation of CWSI and T_c for various irrigation treatments.

has 4.66 and 71.23% (Orta *et al.* 2004), the semi-arid region of Adana, Turkey has 5.43 and 77.63% (Alghory & Yazar 2019), the humid subtropical region of NCP, China has 16.28 and 37.9% (Yuan *et al.* 2004), the Mediterranean region of Shiraz, Iran has 9.3 and 31.96% (Bijanzadeh & Emam 2012), the cold semi-arid region of Bushland, Texas has 0 and 29.68% (Howell *et al.* 1986), and the sub-humid subtropical region of Orissa, India has 14.5 and 72.24% (Kar & Kumar 2010).

The variation in the lower baseline of the wheat crop for other climate regions of the world from the lower baseline at 10 cm of our study area represents a range of 0–16% in slope and 4.9–81.3% in intercept. The variation in the slope of lower baselines from 10 to 100 cm in sub-humid tropical climate of Uttar Pradesh, India bears similarity with the variation in the slope of lower baseline from 10 cm (our study area) to 50 cm case of semi-arid region of Turkey (Orta *et al.* 2004). It can be seen that the lower baselines developed within one experimental location with different sensor location bears less variation when compared to variation from lower baselines of different climate types. For the same crop of wheat, other factors like irrigation type, irrigation treatments, and climate will contribute to a greater change in the lower baselines than the change in distance of the sensor, keeping other factors constant.

These findings underscore the significance of considering climate, irrigation practices, and sensor location (of IRT) in interpreting lower baseline values for effective canopy temperature assessment in crop studies.

3.3. Analysis of CWSI values at distances of 10 and 100 cm

When CWSI values estimated at the observation distances of 10 and 100 cm were compared, it was found that plot 2 had the largest CWSI variation, followed by plot 1, plot 4, and plot 3. CWSI has increased in plot 2 by 36.4% whereas it has decreased in plots 1, 4, and 3 by 21.8, 12.2, and 9.2%, respectively (Figure 5). The CWSI variation follows the same trend across plots as T_c variation (Figure 5). Notably, the T_c bears a positive change from 10 to 100 cm for all plots, whereas CWSI bears a positive change only for plot 2.

Table 2 provides an overview of the mean, minimum, and maximum CWSI values at both 10 and 100 cm observation distances. It is evident that flood-irrigated plots consistently exhibit higher CWSI values. Notably, plot 3 stands out with the highest mean CWSI of 0.40 at the 10 cm IRT distance. In contrast, DI plots maintain mean CWSI values below 0.09 for both 10 and 100 cm distances. As can be seen, the variation of mean CWSI from 10 to 100 cm case for plots 1, 2, 3, and 4 is −0.02, −0.01, −0.03, and −0.04, respectively. The mean CWSI has decreased by 0.025% on average across all treatments.

Furthermore, a closer examination reveals that the minimum CWSI values have shifted slightly. Plots 1, 2, 3, and 4 show changes of −0.01, −0.01, −0.02, and −0.12, respectively, when comparing 10–100 cm distances. Similarly, the maximum CWSI values have experienced alterations of −0.02, +0.02, +0.05, and +0.02 for plots 1, 2, 3, and 4, respectively.

To contextualize our findings, we reference the work of Ru *et al.* (2020) who reported seasonal CWSI values of 0.18, 0.35, and 0.68 for a 10 cm IRT case with various irrigation treatments in grapevines. In contrast, our study yielded seasonal CWSI values of 0.09, 0, 0.40, and 0.33 for plots 1, 2, 3, and 4, respectively, under the 10 cm IRT case.

Our analysis reveals a clear upward trend in CWSI values, with plot 2 exhibiting the lowest stress levels, followed by plot 1, plot 4, and finally plot 3. This trend holds true for both mean and maximum CWSI values at both the 10 and 100 cm observation distances. Conversely, when considering minimum CWSI values, we observe an ascending pattern across the plots, following the sequence of plot 2, plot 1, plot 3, and plot 4. Notably, it is apparent that drip irrigation systems consistently exhibit lower stress levels than flood irrigation systems, regardless of the IRT's location. This underscores the efficacy of drip irrigation in optimizing on-farm water supply and promoting water conservation.

Figure 6 represents the trend of CWSI in all plots for 10 and 100 cm distances over the observation period of the wheat study season. For plot 1, CWSI ranges between −0.10 and 0.30 (10 cm case) and −0.11 and 0.28 (100 cm case). Figure 6(a)

Table 2 | Mean, maximum, and minimum CWSI at 10 and 100 cm for various irrigation treatments

	100 cm			10 cm		
Plots	Mean CWSI	Minimum CWSI	Maximum CWSI	Mean CWSI	Minimum CWSI	Maximum CWSI
1	0.07	−0.11	0.28	0.09	−0.10	0.30
2	−0.01	−0.20	0.12	0.00	−0.19	0.10
3	0.37	−0.09	1.01	0.40	−0.07	0.96
4	0.29	−0.03	0.71	0.33	0.09	0.69

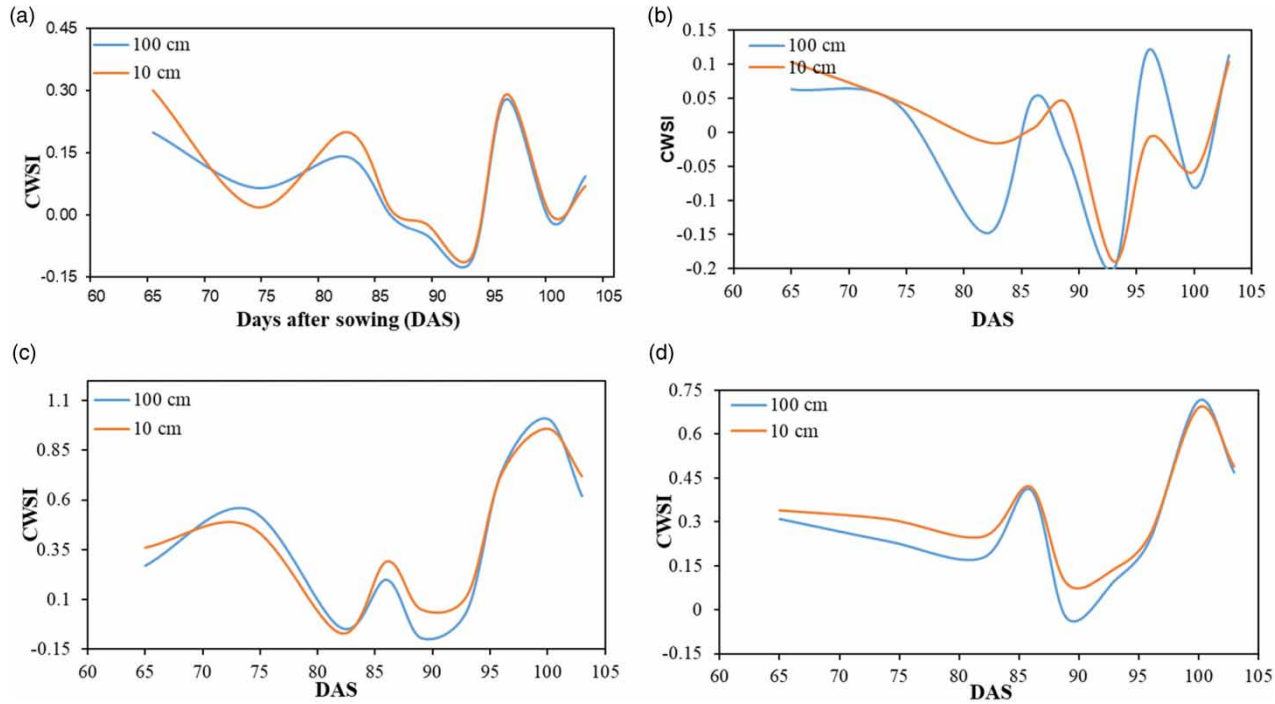

Figure 6 | CWSI trends for observation distances of 10 and 100 cm in various irrigation treatments (a) plot 1, (b) plot 2, (c) plot 3, and (d) plot 4.

depicts the maximal variation in CWSI for plot 1 as a decrease of 0.06 on 82 days after sowing (DAS) and an increase of 0.05 on 74 DAS. CWSI ranges from −0.19 to 0.1 (10 cm case) and −0.20 to 0.12 (100 cm case) in plot 2. Figure 6(b) depicts a maximal variation of 0.13 for 82 DAS and 96 DAS in plot 2. In addition, plot 3 displays the CWSI range as −0.07 to 0.96 (10 cm case) and −0.09 to 1.01 (100 cm case). Figure 6(c) depicts a maximal decrease of 0.14 on DAS 89, followed by a decrease of 0.1 on DAS 103. Similarly, plot 4 shows a CWSI range of 0.09 to 0.69 (10 cm case) and −0.03 to 0.71 (100 cm case). Figure 6(d) indicates that plot 4 reveals a decrease of 0.12 on 89 DAS followed by a decrease of 0.08 on 74 DAS. As the plot with the least amount of water stress, plot 2 exhibits a large number of negative CWSI values and represents non-transpiring conditions the majority of the time. The peaks and valleys of the CWSI trend line for both cases are comparable for plots 1, 3, and 4. Figure 6(b) demonstrates that the maximum and minimum for 10 and 100 cm cases in CWSI evaluation, in relation to days after sowing are not perfectly synchronized. This variation is most evident in the values of T_c and CWSI, which vary by 2.7 and 36.4%, respectively, from 10 to 100 cm cases.

To further investigate the collinearity of CWSI values at 10 and 100 cm, a linear regression analysis was conducted considering all data points (non-averaged) for each irrigation treatment as shown in Figure 7. The results confirm previous observations: Plots 1 and 2, with maximum CWSI variation, have R^2 values of 0.65 and 0.50, respectively, while plots 3 and 4 exhibit higher R^2 values of 0.92 and 0.93, respectively. This analysis underscores the influence of IRT positioning on plots subject to drip irrigation, emphasizing the importance of IRT placement in CWSI assessment using portable IRT devices.

The plots that are subjected to drip irrigation are mostly influenced by the positioning of the IRT. Hence, the examination of IRT's role holds considerable importance in study investigations pertaining to the assessment of CWSI employing portable IRT devices. The authors posit that the lateral uneven wetting observed in drip irrigation resulted in a wider range of T_c values between 10 and 100 cm and consequently CWSI values also.

3.4. Analysis of soil moisture-CWSI relationship for 10 and 100 cm distance

This section presents the findings regarding the relationship between soil moisture depletion (%) and CWSI values, with observations made at two different distances: 10 and 100 cm from the crop canopy. The strength of this relationship is quantified using the determination coefficient (R^2), providing insights into the correlation's robustness. The results demonstrate a

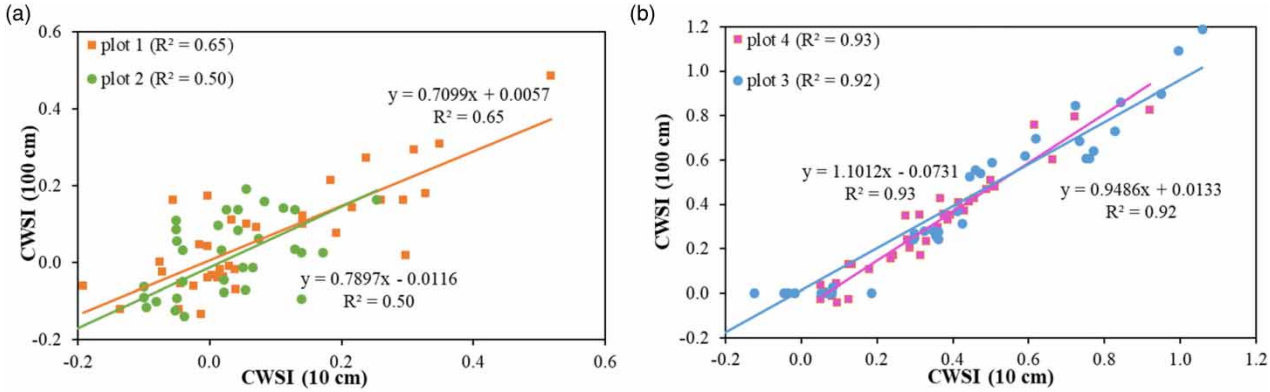

Figure 7 | Linear relationships between CWSI at 10 cm and CWSI at 100 cm for various irrigation treatments of (a) drip systems and (b) flood systems.

compelling correlation between soil moisture depletion and CWSI values at both observation distances. Notably, R^2 values of 0.78 and 0.77 were obtained for the 10 and 100 cm cases, respectively (Figure S1).

To contextualize our results, we refer to analogous studies in the field. For instance, Ru *et al.* (2020) observed a strong relationship ($R^2 = 0.67$) between soil moisture and CWSI when the IRT was positioned at 5–10 cm from the canopy. Similarly, Çolak *et al.* (2021), who positioned the IRT at 100 cm from the quinoa crop, reported an impressive quadratic relationship (R^2 values of 0.897 and 0.997) between soil water content (%) and CWSI during different cropping seasons.

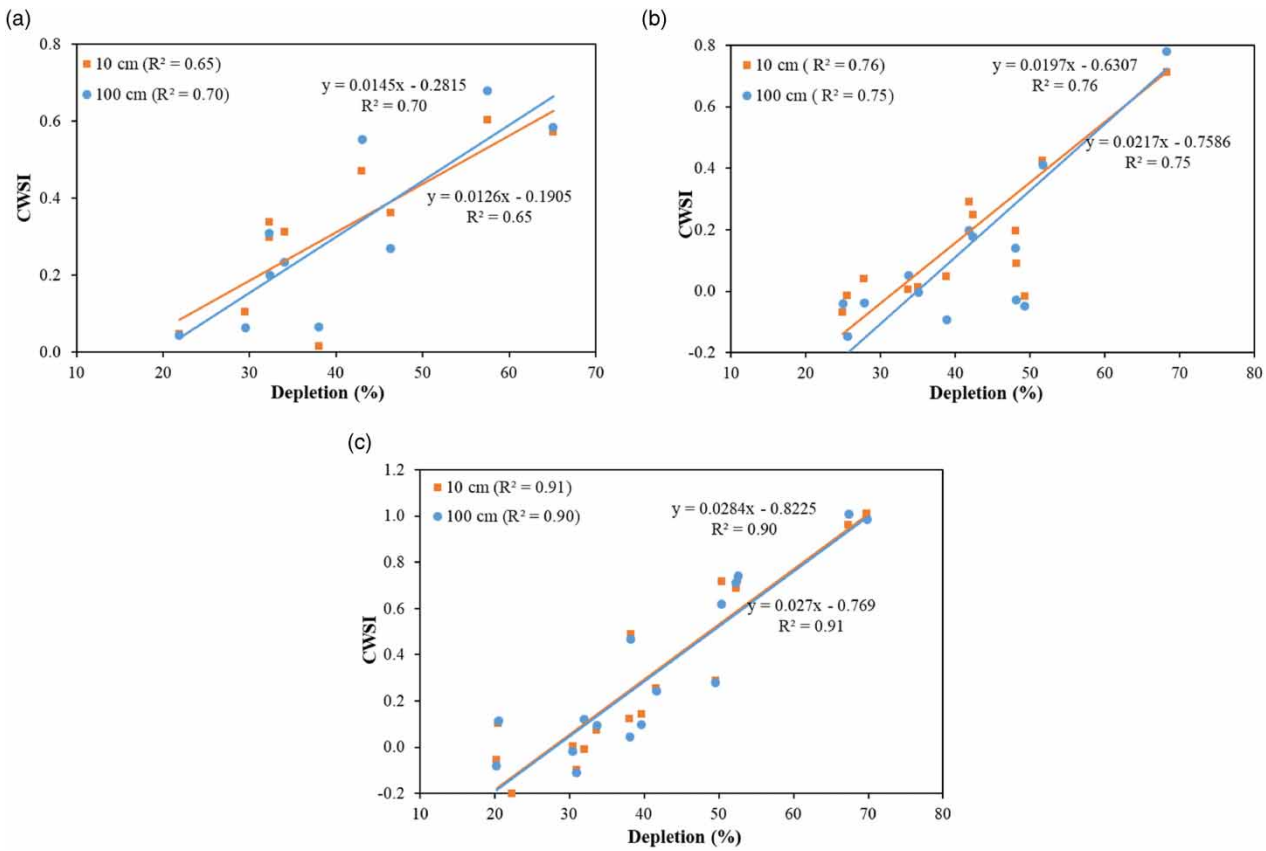

Figure 8 | Linear relationship between CWSI and soil moisture depletion (%) for 10 and 100 cm over growth stages of (a) pre-heading, (b) anthesis, and (c) grain filling.

These findings collectively affirm that CWSI serves as a robust indicator of soil moisture, regardless of the IRT's observation distance.

Moreover, we conducted a granular analysis of the relationship between soil moisture depletion (%) and CWSI across three distinct crop growth stages: pre-heading, anthesis, and grain-filling (Figure 8). Intriguingly, our results reveal an evolving relationship as the crop matures. Specifically, during the pre-heading stage, R^2 values were 0.65 (10 cm) and 0.70 (100 cm) (Figure 8(a)). The anthesis stage exhibited R^2 values of 0.76 (10 cm) and 0.75 (100 cm) (Figure 8(b)). However, the most striking correlation emerged during the grain-filling stage, with R^2 values of 0.91 (10 cm) and 0.90 (100 cm) (Figure 8(c)). This suggests that as the crop progresses through growth stages, the CWSI increasingly reflects plant stress associated with soil moisture depletion. This finding underscores the significance of the grain-filling stage in understanding the relationship between CWSI and soil moisture, particularly in wheat crop studies.

Crucially, our research confirms that the location of the IRT sensor, whether at 10 or 100 cm, does not substantially affect the moisture and CWSI relationship. This highlights the robustness and practical applicability of our findings.

4. CONCLUSION

In this study, we conducted field experiments on wheat crops during the 2021–2022 season, focusing on controlled irrigation treatments. Our research was driven by the need for a standardized approach to canopy temperature (T_c) observation using infrared thermometers (IRT). To address this gap, we systematically evaluated CWSI using T_c observations at two distinct distances from the canopy: 10 and 100 cm. This allowed us to compare T_c values, CWSI, and lower baselines for both cases.

Our analysis revealed several key insights. Notably, DI plots (2 and 1) exhibited the highest T_c and CWSI variations, with plot 2 experiencing a maximum T_c variation of 2.71% and a CWSI variation of 36.4%. Plot 1 showed a T_c variation of 2.1% and a CWSI variation of 21.9%. In contrast, flood-irrigated plots (3 and 4) demonstrated lower variations in T_c (0.65 and 0.86%) and CWSI (9.2 and 12.2%). Our findings also underscored the influence of the crop development stage on IRT placement. While most previous studies maintained a constant IRT distance throughout all growth phases, we observed that T_c sensitivity to IRT location increased during the grain-filling stage, particularly for DI plots. This increase was significant, with T_c values in plot 1 and plot 2 rising by 2.4 and 3.6%, respectively, when shifting the IRT from 10 to 100 cm.

While drip irrigation offers higher water use efficiency and precise water distribution compared to flood irrigation (Yadav *et al.* 2022), as indicated by lower stress values in plots 1 and 2 (DI) compared to plots 3 and 4 (flood-irrigated), we found that the drip system was more sensitive to IRT location changes. This increased sensitivity may be attributed to uneven lateral soil wetting and the potential interference of drip pipelines in the background when IRT readings were taken at 100 cm. The trend for CWSI between IRT at 10 and 100 cm cases is that plot 3 has the highest CWSI values, followed by plot 4, plots 1 and 2. CWSI is 0.40 (10 cm) and 0.37 (100 cm) for plot 3, 0.33 (10 cm) and 0.29 (100 cm) for plot 4, 0.09 (100 cm) and 0.07 (10 cm) for plot 1, and 0 (10 cm) and −0.01 (100 cm) for plot 2.

Furthermore, our study highlighted the importance of understanding the relationship between lower baselines and the spatial resolution of IRT. We found that $T_c - T_a$ and VPD exhibited a stronger correlation at 10 cm ($R^2 = 0.83$) than at 100 cm ($R^2 = 0.77$). For precise lower baselines, our results suggest that the IRT should be positioned at 10 cm from the crop surface. Importantly, we found that the spatial resolution of the IRT had no significant effect on the correlations between soil moisture and CWSI at any crop stage.

In conclusion, our study has shed light on the influence of IRT observation distance on empirical CWSI values, particularly in the context of different irrigation systems. We observed that drip-irrigated plots were more responsive to changes in IRT location, while flood-irrigated plots exhibited smaller CWSI variations. It is evident that CWSI values can vary based on the scale of analysis and the specific IRT distance employed. Further research opportunities exist to explore the correlation between IRT distance from the canopy and the optimal arrangement of drip pipe networks, aiming to minimize the impact of IRT distance on T_c and CWSI. These findings have practical implications for irrigation management, offering insights into the optimal use of remote sensing devices for improved crop stress monitoring and water resource utilization in agriculture.

ACKNOWLEDGEMENTS

The authors would like to acknowledge the financial support of an ongoing research project for carrying out this research work. The project titled 'Development of AI-Based DSS for Improved Crop Water Use Efficiency under Regulated Deficit

Drip Irrigation Regime in The Backdrop of Climate Change' (DST/DMD, EWO/WTI/2K19/EWFH/2019/277(g)) is funded by Department of Science and Technology, Government of India.

FUNDING

This work was funded by Department of Science and Technology, Government of India under the project titled 'Development of AI-Based DSS for Improved Crop Water Use Efficiency under Regulated Deficit Drip Irrigation Regime in The Backdrop of Climate Change'- DST/DMD, EWO/WTI/2K19/EWFH/2019/277(g).

DATA AVAILABILITY STATEMENT

All relevant data are included in the paper or its Supplementary Information.

CONFLICT OF INTEREST

The authors declare there is no conflict.

REFERENCES

Adeyemi, O., Grove, I., Peets, S., Domun, Y. & Norton, T. 2018 Dynamic modelling of the baseline temperatures for computation of the crop water stress index (CWSI) of a greenhouse cultivated lettuce crop. *Computers and Electronics in Agriculture* **153**, 102–114. https://doi.org/10.1016/j.compag.2018.08.009.

Akuraju, V. R., Ryu, D. & George, B. 2021 Estimation of root-zone soil moisture using crop water stress index (CWSI) in agricultural fields. *GIScience and Remote Sensing* **58** (3), 340–353. https://doi.org/10.1080/15481603.2021.1877009.

Alderfasi, A. & Nielsen, D. 2001 Use of crop water stress index for monitoring water status and scheduling irrigation in wheat. *Agricultural Water Management* **47**, 69–75. https://www.sciencedirect.com/science/article/pii/S0378377400000962.

Alghory, A. & Yazar, A. 2019 Evaluation of crop water stress index and leaf water potential for deficit irrigation management of sprinkler-irrigated wheat. *Irrigation Science* **37**, 61–77. https://link.springer.com/content/pdf/10.1007/s00271-018-0603-y.pdf.

Bellvert, J., Zarco-Tejada, P. J., Girona, J. & Fereres, E. 2014 Mapping crop water stress index in a 'Pinot-noir' vineyard: Comparing ground measurements with thermal remote sensing imagery from an unmanned aerial vehicle. *Precision Agriculture* **15** (4), 361–376. https://doi.org/10.1007/S11119-013-9334-5.

Bijanzadeh, E. & Emam, Y. 2012 Evaluation of crop water stress index, canopy temperature and grain yield of five Iranian wheat cultivars under late season drought stress. *Journal of Plant Physiology and Breeding* **2** (1), 23–33. http://breeding.tabrizu.ac.ir/pdf_3087_ee37a3789790843c7d9127647974250c.html.

Çolak, Y. B., Yazar, A., Çolak, İ., Akça, H. & Duraktekin, G. 2015 Evaluation of crop water stress index (CWSI) for Eggplant under varying irrigation regimes using surface and subsurface drip systems. In: *Agriculture and Agricultural Science Procedia*, Vol. 4, pp. 372–382. https://doi.org/10.1016/J.AASPRO.2015.03.042.

Çolak, Y., Yazar, A., Alghory, A. & Tekin, S. 2021 Evaluation of crop water stress index and leaf water potential for differentially irrigated quinoa with surface and subsurface drip systems. *Irrigation Science* **39** (1), 81–100. https://doi.org/10.1007/S00271-020-00681-4.

DeJonge, K. C., Taghvaeian, S., Trout, T. J. & Comas, L. H. 2015 Comparison of canopy temperature-based water stress indices for maize. *Agricultural Water Management* **156**, 51–62.

Ehlers, J. H. 1915 The temperature of leaves of *Pinus* in winter. *J .Bot.* https://doi.org/10.1002/j.1537-2197.1915.tb09390.x

Erdem, Y., Arin, L., Erdem, T., Polat, S., Deveci, M., Okursoy, H. & Gültaş, H. T. 2010 Crop water stress index for assessing irrigation scheduling of drip irrigated broccoli (*Brassica oleracea* L. var. *italica*). *Agricultural Water Management* **98** (1), 148–156. https://doi.org/10.1016/j.agwat.2010.08.013.

Garrot Jnr, D. J., Ottman, M. J., Fangmeier, D. D. & Husman, S. H. 1994 Quantifying wheat water stress with the crop water stress index to schedule irrigations. *Agronomy Journal* **86** (1), 195–199. https://doi.org/10.2134/agronj1994.00021962008600010034x.

Gölgül, İ., Kırnak, H. & Ali İrik, H. 2022 Yield components and crop water stress index (CWSI) of mung bean grown under deficit irrigations. *Gesunde Pflanzen*. https://doi.org/10.1007/s10343-022-00698-z.

Gontia, N. K. & Tiwari, K. N. 2008 Development of crop water stress index of wheat crop for scheduling irrigation using infrared thermometry. *Agricultural Water Management* **95**, 1144–1152. https://doi.org/10.1016/j.agwat.2008.04.017.

Haghverdi, A., Reiter, M., Singh, A. & Sapkota, A. 2021 Hybrid bermudagrass and tall fescue turfgrass irrigation in central California: Ii. assessment of NDVI, CWSI, and canopy temperature dynamics. *Agronomy* **11** (9). https://doi.org/10.3390/agronomy11091733.

Han, M., Zhang, H., DeJonge, K. C., Comas, L. H. & Gleason, S. 2018 Comparison of three crop water stress index models with sap flow measurements in maize. *Agricultural Water Management* **203**, 366–375. https://doi.org/10.1016/j.agwat.2018.02.030.

Howell, T. A., Musick, J. T. & Tolk, J. A. 1986 Canopy temperature of irrigated winter wheat. *Transactions of the American Society of Agricultural Engineers* **29** (6), 1692–1698. https://doi.org/10.13031/2013.30375.

Idso, S. B. 1982 Non-water-stressed baselines: A key to measuring and interpreting plant water stress. *Agricultural Meteorology* **27**, 59–70.

Idso, S. B., Jackson, R. D., Pinter, P. J., Reginato, R. J. & Hatfield, J. L. 1981 Normalizing the stress-degree-day parameter for environmental variability. *Agricultural Meteorology* **24**, 45–55.

Irandoust, T. & Bijanzadeh, E. 2018 Effect of two irrigation regimes on crop water stress index and yield and yield components of Triticale (X Triticosecale Wittmack) Cultivars. *Journal of Plant Process and Function* **6** (22), 15–22.

Jackson, R. D., Reginato, R. J. & Idso, S. B. 1977 Wheat canopy temperature: A practical tool. *Water Resources Research* **13** (3), 651–655.

Jackson, R. D., Idso, S. B., Reginato, R. J. & Pinter, P. J. 1981 Canopy temperature as a crop water stress indicator. *Water Resources Research* **17** (4), 1133–1138.

Jalali-Farahani, H. R., Slack, D. C., Kopec, D. M. & Matthias, A. D. 1993 Crop water stress index models for bermudagrass turf: A comparison. *Agronomy Journal* **85** (6), 1210–1217. https://doi.org/10.2134/agronj1993.00021962008500060022x.

Jamshidi, S., Zand-Parsa, S. & Niyogi, D. 2021 Assessing crop water stress index of citrus using in-situ measurements, landsat, and sentinel-2 data. *International Journal of Remote Sensing* **42** (5), 1893–1916. https://doi.org/10.1080/01431161.2020.1846224.

Kar, G. & Kumar, A. 2007 Surface energy fluxes and crop water stress index in groundnut under irrigated ecosystem. *Agricultural and Forest Meteorology* **146**, 94–106. https://doi.org/10.1016/j.agrformet.2007.05.008.

Kar, G. & Kumar, A. 2010 Energy balance and crop water stress in winter maize under phenology-based irrigation scheduling. *Irrigation Science* **28** (3), 211–220. https://doi.org/10.1007/s00271-009-0192-x.

Khorsand, A., Rezaverdinejad, V., Asgarzadeh, H. & Heris, A. M. 2021 Linking plant and soil indices for water stress management in black gram. *Nature Scientific Reports* **11** (869), 1–19. https://doi.org/10.1038/s41598-020-79516-3.

King, B. A., Tarkalson, D. D., Sharma, V. & Bjorneberg, D. L. 2021 Thermal crop water stress index base line temperatures for sugarbeet in arid western U.S. *Agricultural Water Management* **243**. https://doi.org/10.1016/j.agwat.2020.106459.

Kirnak, H., Irik, H. A. & Unlukara, A. 2019 Potential use of crop water stress index (CWSI) in irrigation scheduling of drip-irrigated seed pumpkin plants with different irrigation levels. *Scientia Horticulturae* **256**. https://doi.org/10.1016/j.scienta.2019.108608.

Kottek, M., Grieser, J., Beck, C., Rudolf, B. & Rubel, F. 2006 World map of the Köppen-Geiger climate classification updated. *Meteorologische Zeitschrift* **15** (3), 259–263. https://doi.org/10.1127/0941-2948/2006/0130.

Kumar, N., Poddar, A., Shankar, V., Ojha, C. S. P. & Adeloye, A. J. 2019 Crop water stress index for scheduling irrigation of Indian mustard (*Brassica juncea*) based on water use efficiency considerations. *Journal of Agronomy and Crop Science* **206** (1), 148–159. https://doi.org/10.1111/JAC.12371.

Kumar, N., Adeloye, A. J., Shankar, V. & Rustum, R. 2020 Neural computing modelling of the crop water stress index. *Agricultural Water Management* **239**. https://doi.org/10.1016/j.agwat.2020.106259.

Li, L., Nielsen, D. C., Yu, Q., Ma, L. & Ahuja, L. R. 2010 Evaluating the crop water stress index and its correlation with latent heat and CO_2 fluxes over winter wheat and maize in the North China plain. *Agricultural Water Management* **97** (8), 1146–1155. https://doi.org/10.1016/j.agwat.2008.09.015.

Miller, E. & Saunders, A. 1923 Some observations on the temperature of the leaves of crop plants. *Journal of Agricultural Research*. Available from: https://ci.nii.ac.jp/naid/10016223032/.

Orta, A. H., Başer, I., Şehirali, S., Erdem, T. & Erdem, Y. 2004 Use of infrared thermometry for developing baseline equations and scheduling irrigation in wheat. *Cereal Research Communications* **32** (3), 363–370. https://doi.org/10.1007/BF03543322.

Paltineanu, C., Septar, L. & Moale, C. 2013 Crop water stress in peach orchards and relationships with soil moisture content in a Chernozem of Dobrogea. *Journal of Irrigation and Drainage Engineering* **139** (1), 20–25. https://doi.org/10.1061/(ASCE)IR.1943-4774.0000492.

Payero, J. O. & Irmak, S. 2006 Variable upper and lower crop water stress index baselines for corn and soybean. *Irrigation Science* **25** (1), 21–32. https://doi.org/10.1007/s00271-006-0031-2.

Romero-Trigueros, C., Bayona Gambín, J. M., Nortes Tortosa, P. A., Alarcón Cabañero, J. J. & Nicolás, E. N. 2019 Determination of crop water stress index by infrared thermometry in grapefruit trees irrigated with saline reclaimed water combined with deficit irrigation. *Remote Sensing* **11** (7), 1–23. https://doi.org/10.3390/rs11070757.

Ru, C., Hu, X., Wang, W., Ran, H., Song, T. & Guo, Y. 2020 Evaluation of the crop water stress index as an indicator for the diagnosis of grapevine water deficiency in greenhouses. *Horticulturae* **6** (86), 86. https://doi.org/10.3390/horticulturae6040086.

Shankar, V., Hari Prasad, K. S., Ojha, C. S. P. & Govindaraju, R. S. 2013 Optimizing water use in irrigation – a review. *Journal of the Indian Institute of Science* **93** (2), 209–226.

Shellie, K. C. & King, B. A. 2020 Application of a daily crop water stress index to deficit irrigate Malbec grapevine under semi-arid conditions. *Agriculture* **10** (492), 1–17.

Sneha, C., Santhoshkumar, A. & Sunil, K. 2013 Quantifying water stress using crop water stress index in mahogany (Swietenia macrophylla King) seedlings. *Current Science* **104** (3), 348–351.

Stegman, E. C. & Soderlund, M. 1992 Irrigation scheduling of spring wheat using infrared thermometry. *Transaction of the American Society of Agricultural Engineers (ASAE)* **35** (1), 143–153.

Stockle, C. O. & Dugas, W. A. 1992 Evaluating canopy temperature-based indices for irrigation scheduling. *Irrigation Science* **13** (1), 31–37. https://doi.org/10.1007/BF00190242.

Taghvaeian, S., Chávez, J. L. & Hansen, N. C. 2012 Infrared thermometry to estimate crop water stress index and water use of irrigated maize in northeastern Colorado. *Remote Sensing* **4** (11), 3619–3637. https://doi.org/10.3390/RS4113619.

Taghvaeian, S., Comas, L., DeJonge, K. C. & Trout, T. J. 2014 Conventional and simplified canopy temperature indices predict water stress in sunflower. *Agricultural Water Management* **144**, 69–80. https://doi.org/10.1016/J.AGWAT.2014.06.003.

The World Bank Report 2020 *Water in Agriculture*.

United Nations (UN) 2022 *The Sustainable Development Goals Report*.

Usman, M., Ahmad, A., Ahmad, S. & Irshad, M. 2009 Development and application of crop water stress index for scheduling irrigation in cotton (*Gossypium hirsutum* L.) under semiarid environment. *J Food Agric.* Available from: https://www.academia.edu/download/38171180/352.pdf.

Yadav, A., Sharma, N., Upreti, H. & Das Singhal, G. 2022 Techno-economic analysis of irrigation systems for efficient water use in the backdrop of climate change. *Current Science* **122** (6), 664–672.

Yuan, G., Luo, Y., Sun, X. & Tang, D. 2004 Evaluation of a crop water stress index for detecting water stress in winter wheat in the North China Plain. *Agricultural Water Management* **64**, 29–40. https://doi.org/10.1016/S0378-3774(03)00193-8.

First received 28 June 2023; accepted in revised form 19 November 2023. Available online 28 November 2023